This is the author's version of an article that has been published in this journal. Changes were made to this version by the publisher prior to publication.
The final version of record is available at http://dx.doi.org/10.1109/JSEN.2018.2849873

A High-Precision and High-Bandwidth MEMS-based Capacitive Accelerometer[1]

Alexander Utz, Christian Walk, Alexander Stanitzki, Mir Mokhtari, Michael Kraft, Rainer Kokozinski

***Abstract*—In this paper, we present a capacitive, MEMS-based accelerometer comprising an ultra-low noise CMOS integrated readout-IC and a high-precision bulk micro machined sensing element. The resulting accelerometer reaches an acceleration equivalent noise of only 200 ng/√Hz, which makes it suitable for seismic measurement that require noise levels significantly below 1 µg/√Hz. Additionally, a high bandwidth of more than 5 kHz was achieved, which also makes the presented sensor system applicable for high-frequency measurements, e.g. in predictive maintenance applications for rotating machinery. The design of the sensing element and readout IC is presented in detail and measurement results are shown which demonstrate the performance of the sensor system.**

***Index Terms*—capacitive sensing, low-noise, accelerometer, MEMS**

I. Introduction

Capacitive sensors are widely used for the accurate measurement of physical quantities such as pressure, acceleration or orientation. In contrast to sensors, which are composed of discrete mechanical elements, MEMS (micro-electro-mechanical system) based solutions have suffered, and still suffer, from a significantly increased noise level and thus reduced measurement performance [1]. A mechanical noise source within the MEMS sensing element itself is the Brownian noise induced by thermal motion of the air atoms inside the MEMS package. There are multiple methods for reducing the MEMS noise and increasing the measurement dynamic range (DR), one of them is vacuum sealing of the sensing structure [2]. Applications such as seismic measurement or highly sensitive vibration detection, e.g. crucial in earthquake early detection or vibration monitoring of buildings, require noise levels significantly below 1 µg/√Hz. Current sensor MEMS reach noise levels considerably lower than that, which allows their use in such applications.

The readout IC's (ROIC) electrical noise adds to the MEMS' mechanical noise. For highly optimized MEMS sensors with high sensitivity and low mechanical noise contribution the ROIC becomes dominant. Therefore, the reduction of input referred electrical noise becomes the most important parameter in the ROIC design for such MEMS sensors.

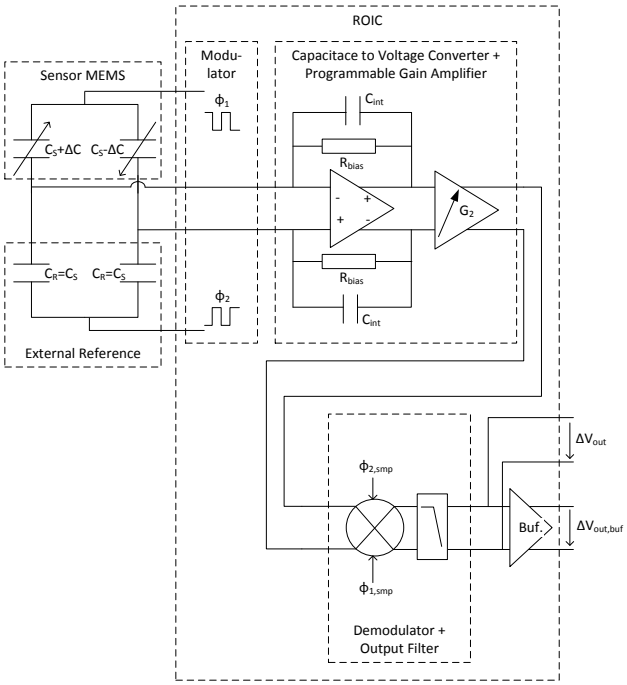

Fig. 1. Block diagram of the presented accelerometer

A complete, high sensitivity, low noise acceleration measurement system containing an ultra-low noise ROIC from Fraunhofer IMS and a MEMS sensing element from Mir Enterprises was developed. The achieved performance is

This paragraph of the first footnote will contain the date on which you submitted your paper for review. It will also contain support information, including sponsor and financial support acknowledgment. For example, "This work was supported in part by the U.S. Department of Commerce under Grant BS123456".

A. Utz, C. Walk, A. Stanitzki and R. Kokozinski are with Fraunhofer Institute for Microelectronic Circuits and Systems (IMS), Finkenstr. 61, 47057 Duisburg, Germany (e-mail: Alexander.Utz@ims.fraunhofer.de; Christian.Walk@ims.fraunhofer.de; Alexander.Stanitzki@ims.fraunhofer.de; Rainer.Kokozinski@ims.fraunhofer.de)

M. Mokhtari is with Mir Enterprises Limited, 173c Goldhurst Terrace, Hampstead, London, NW6 3ES, United Kingdom (e-mail: mokhtari@mir-enterprises.com; web: www.mir-enterprises.com)

M. Kraft is with Department of Electrical Engineering – MICAS, KU Leuven, Kasteelpark Arenberg 10, 3001 Leuven, Belgium (e-mail: michael.kraft@kuleuven.be)

R. Kokozinski is with Department of Electronic Components and Circuits, University of Duisburg-Essen, Bismarckstr. 81, 47057 Duisburg, Germany (e-mail: rainer.kokozinski@uni-due.de)

[1] An earlier version of this paper was presented at the IEEE Sensors 2017 Conference and was published in its Proceedings: http://ieeexplore.ieee.org/document/8233981/?reload=true

Copyright (c) 2018 IEEE. Personal use is permitted. For any other purposes, permission must be obtained from the IEEE by emailing pubs-permissions@ieee.org.

This is the author's version of an article that has been published in this journal. Changes were made to this version by the publisher prior to publication.
The final version of record is available at http://dx.doi.org/10.1109/JSEN.2018.2849873

much better than that of similar systems reported during the last years [1], [3] and at least equal to systems which apply vacuum sealing of the sensing element [4], which is not necessary in our case. Both ROIC and sensing element were designed with focus on low noise and manufacturability in standard compatible processes. Fig. 1 shows a simplified block diagram of the developed accelerometer. The design and implementation of the ROIC and sensing element will be discussed in Sec. II and measurement results, which proof the claimed performance, will be presented in Sec. III.

II. Accelerometer Architecture and Design

The two main parts of the presented sensor system are the analog ROIC and the capacitive sensing element. Both components will be discussed in detail in this section.

A. Capacitive sensing element

The MEMS sensing element is a typical capacitive device with in-plane, single axis sensitivity fabricated in an SOI (silicon on insulator) process on an eight inch wafer with a 100 µm structural layer. The principle of the fabrication process is described in detail in [5]; it relies on removing the handle wafer underneath the active device area by a process step in which the wafer is immersed in HF vapour. The HF vapour etches the silicon dioxide of the BOX (buried oxide layer) in areas where it can reach it; these are defined by two DRIE (deep reactive ion etching) steps performed first from the front and then from the back side. In this way the chips are separated without dicing and concurrently the handle wafer underneath the active area is freed, so that is can drop out in a controlled way. The yield of the fabrication process is very high, close to 100 %.

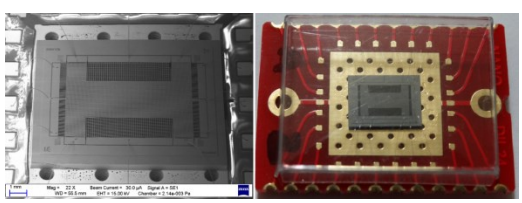

Fig. 2. *SEM image and photograph of the MEMS sensing element*

The MEMS has comb fingers on all sides of the H-shaped proof mass. The comb fingers on the left and right of the proof mass can be used for closed loop operation. The open loop comb fingers attached to the top and bottom of the proof mass form the sense capacitors with a nominal value of approximately 10 pF. The proof mass has an outline of 6605 µm x 4139 µm (B x H) and a thickness h of 50 µm. As it contains many holes due to the production process, the overall silicon density D is reduced to 54.67 %. Small features like the suspensions and curved edges add an extra amount of area δA of $9.79 \cdot 10^5$ µm^2. With the specific density of silicon ρ_{Si} of 2.336 g/cm^3, the total mass of the proof mass can be calculated as $M=(B \cdot H \cdot D + \delta A) \cdot h \cdot \rho_{Si}$ and yields 1.86 mg. The large proof mass leads to a high sensitivity in conjunction with a very low noise floor. The total noise equivalent acceleration (TNEA) can be calculated from the sensor's damping factor D and it's mass M (or, which is equivalent, its resonant frequency ω_T, quality factor Q and mass M) as [6], [7]

$$TNEA = \frac{\sqrt{4k_BTD}}{M} = \sqrt{\frac{4k_BT\omega_T}{QM}}. \quad (1)$$

The quality factor Q for these types of MEMS is 8.95 and its natural frequency ω_T 237 Hz (respectively 1489 rad/s).

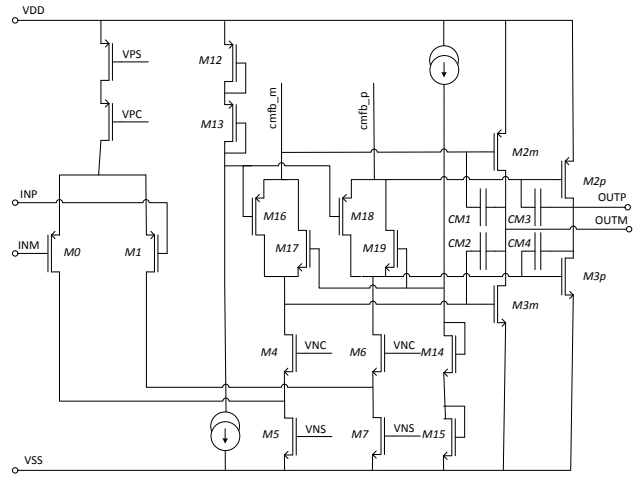

Fig. 3. *Architecture of the class AB amplifier*

Both values have been calculated with the aid of CAD tools and are functions of the mass of the proof mass and the spring constant of the suspension, which, again, result from the sensor geometry and the elastic modulus of silicon. The resulting theoretical Brownian noise floor of the sensing element is 124 ng/$\sqrt{\text{Hz}}$. The change in capacitance per 1 g (=9.81 m/s^2) is about 0.55 pF, which provides the input signal to the ASIC. The sensing element was packaged under atmospheric pressure. The main important parameters of the sensing element are summarized in Table 1. Fig. 2 shows a scanning electron microscope (SEM) image of the chip (left) and a photograph of the chip mounted and wire-bonded on a carrier printed circuit board.

B. Analog ROIC

The sensing element is connected via a fully differential four-wire interface to the ROIC as shown in Fig.1. The core of the readout circuit is a two-stage, fully differential, chopper-stabilized amplifier [8]. The first stage performs the actual capacitance to voltage (C/V) conversion and the second stage provides four programmable gain settings. This is achieved by one fixed and two binary weighted capacitors in the feedback loop of the second stage. The actual gain can be selected by two primary inputs of the chip. The feedback capacitor of the first stage C_{int}, together with the input differential capacitance ΔC of the sensing element, determines the overall closed loop voltage gain of the amplifier stage. The excitation voltage is a square wave with constant amplitude of V_{DD} (i.e. 5 V).

The amplifier stages are followed by the demodulator, which transforms the carrier based signal generated by the square wave excitation voltage back into the baseband and vice versa shifts any accumulated low-frequency noise from the baseband to the carrier frequency. High frequency noise components are eliminated by the final low-pass filter. This

Copyright (c) 2018 IEEE. Personal use is permitted. For any other purposes, permission must be obtained from the IEEE by emailing pubs-permissions@ieee.org.

This is the author's version of an article that has been published in this journal. Changes were made to this version by the publisher prior to publication.
The final version of record is available at http://dx.doi.org/10.1109/JSEN.2018.2849873

filter is realized as passive RC low-pass to avoid the generation of additional 1/f-noise in the signal path. The -3 dB bandwidth of the filter is 80 kHz. The introduced phase shift is negligible within the frequency range of the overall accelerometer. An output buffer allows driving high resistive loads.

The main design goal for the presented ROIC was measurement accuracy, i.e. low noise. The noise induced by the circuit architecture presented in Fig. 1 can be split into noise coming from the operational amplifier itself and the feedback network and additional noise generated by the output

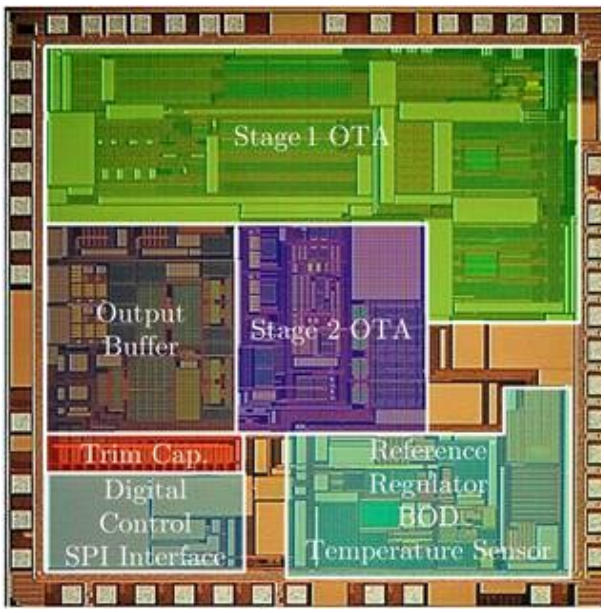

Fig. 4. *Photograph of the chip*

filter. For low frequencies flicker noise components are dominant over the thermal noise ones [9]. The amount and shape of flicker noise introduced is technology and operating point dependent. To allow accurate low frequency measurements, it is crucial to effectively reduce this influence by adequate circuit design techniques. For this reason, the C/V converter was implemented as a chopper amplifier [10], [11]. The total noise power of a chopper amplifier (including the feedback network) can be calculated as [10], [12]

$$v_{nc2v}^2 = \left[\gamma_n \cdot \frac{16}{3}\frac{k_B T}{g_{m0}} \cdot \left(1 + \frac{17 f_k}{2\pi^2 f_{chop}}\right) \cdot \eta\right]_{Amplifier} \cdot (1 + G_1)^2 + \left[\frac{8 k_B T R_{bias}}{1 + 4\pi^2 R_{bias}^2 C_{int}^2 f_{chop}^2}\right]_{Feedback}, \quad (2)$$

where γ_n is the noise excess factor, k_B the Boltzmann constant, T the absolute Temperature, g_{m0} the transconductance of the input transistors, f_k the flicker noise corner frequency, and f_{chop} the chopping frequency. η is a complexity factor which takes into account all noise sources additional to the input differential pair. It will be derived for the chosen amplifier architecture later on. γ_n is assumed to be in the order of 1.5 for the specific input stage transistors operating in moderate inversion [13]. G_1 is the gain of the first stage set by the integration capacitor C_{int}, the differential sensor capacitance C_s, and the parasitic capacitance C_p to $G_1=(2C_s+C_p)/C_{int}$ [14].

With maximum gain in the first amplifier stage and only minimal gain in the second stage, the overall electrical output noise is dominated by the noise of the first stage [15]. From (2) it becomes obvious, that the main parameters for noise reduction are the chopping frequency f_{chop} and the transconductance g_{m0} of the input stage. The flicker noise corner frequency f_k depends on the actual transistor area and technology dependent parameters. For the actual transistor sizing chosen in this design in combination with the 0.35 µm CMOS technology used in this work, it is about 25 kHz. The chopping frequency for the C/V conversion stage has to be chosen so that the second term in the parenthesis of (2) becomes much smaller than 1 and the resulting demands on the OP-Amp design towards slew rate and bandwidth is still realistic.

For the two above reasons, a chopping frequency of 833 kHz was chosen. After demodulation, the flicker noise

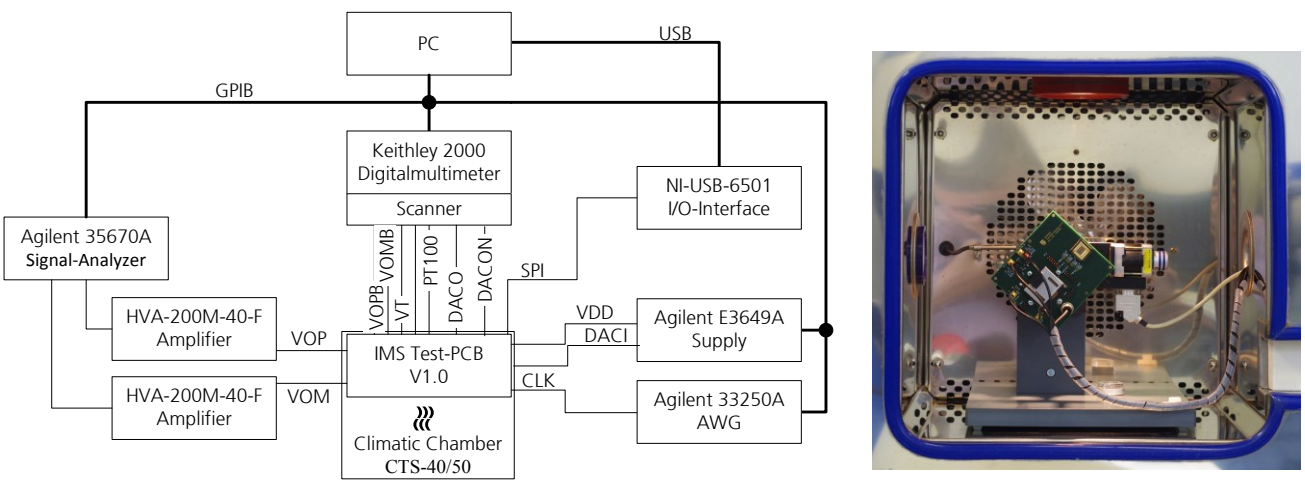

Fig. 5. *Block diagram (left) and Photograph (right) of the automated test chamber*

Copyright (c) 2018 IEEE. Personal use is permitted. For any other purposes, permission must be obtained from the IEEE by emailing pubs-permissions@ieee.org.

This is the author's version of an article that has been published in this journal. Changes were made to this version by the publisher prior to publication.
The final version of record is available at http://dx.doi.org/10.1109/JSEN.2018.2849873

power is shifted from the baseband to the modulation frequency at 833 kHz. To filter out these components, the final output filter band-limits the output signal. The resulting -3 dB bandwidth of the ROIC is 51 kHz. The contribution of flicker noise to the total output noise is thus reduced to a negligible amount.

For the operational amplifiers a fully differential two-stage folded cascode architecture was selected with a push-pull output stage operating in class AB mode. The simplified circuit is shown in Fig. 3 (the additional amplifier for common mode feedback regulation was omitted for simplicity here). The folded cascode input stage allows larger V_{DS} for the differential pair at a fixed 5 V supply voltage and the push-pull output stage isolates the output from the capacitive load, which varies with the selected system gain and depends on the nominal sensor capacitance. The bandwidth of both amplifiers is 200 MHz. A detailed description of the OTA architecture and parameters, including the common mode feedback amplifier, is given in [14].

As can be seen from (2), the transconductance g_{n0} of the transistors of the input differential pair has to be maximized to gain optimal noise performance. To achieve this, a huge W/L ratio of 23296/0.36 together with a bias current of 50 mA was chosen. The resulting g_{m0} is 130 mA/V. Significant contributions to the overall amplifier noise, additional to the input differential pair, is induced by the current source transistor pair M5–M7. The noise current of these transistors propagates directly to the amplifiers output. Thus, the complexity factor η introduced in (2) can be calculated as

$$\eta = 1 + \frac{g_{m5}}{g_{m0}} \tag{3}$$

and is 1.38 for the first stage amplifier (M5 and M7 are equally sized and have the same contribution). The input referred noise of the complete ROIC is then below 50 zF/$\sqrt{\text{Hz}}$.

Fig. 4 shows a photograph of the developed ASIC. The total chip area is 3.5 mm x 3.5 mm. The output of the low-pass filter is directly connected to pads and also fed into an output buffer which is realized as an instrumentation amplifier to drive high resistive loads. A bandgap reference provides an absolute voltage reference for supply regulation and brown out detection. An internal LDO generates the 3.3 V supply for this blocks from the externally supplied 5 V V_{DD}. The integrated brown out detection puts the chip into reset state if the supply voltage falls below a critical limit.

TABLE I
ACCELEROMETER SYSTEM PARAMETERS

Parameter	Value
ROIC	
Electrical noise floor	46.75 zF/$\sqrt{\text{Hz}}$
Sensitivity	1.37 - 5.44 V/pF (selectable)
Bandwidth	51 kHz
MEMS sensing element	
Brownian noise floor	124 ng/$\sqrt{\text{Hz}}$
Nominal capacitance	10 pF
Mass of proof mass	1.86 mg
Natural frequency	237 Hz
Sensitivity	0.55 pF/g
Overall device size	7x9x0.6 mm^3
Accelerometer	
Sensitivity	0.70 – 2.67 V/g (selectable)
Measurement range	±1.25 g - ±5 g (selectable)
Noise floor	216 ng/$\sqrt{\text{Hz}}$
Bandwidth	5 kHz

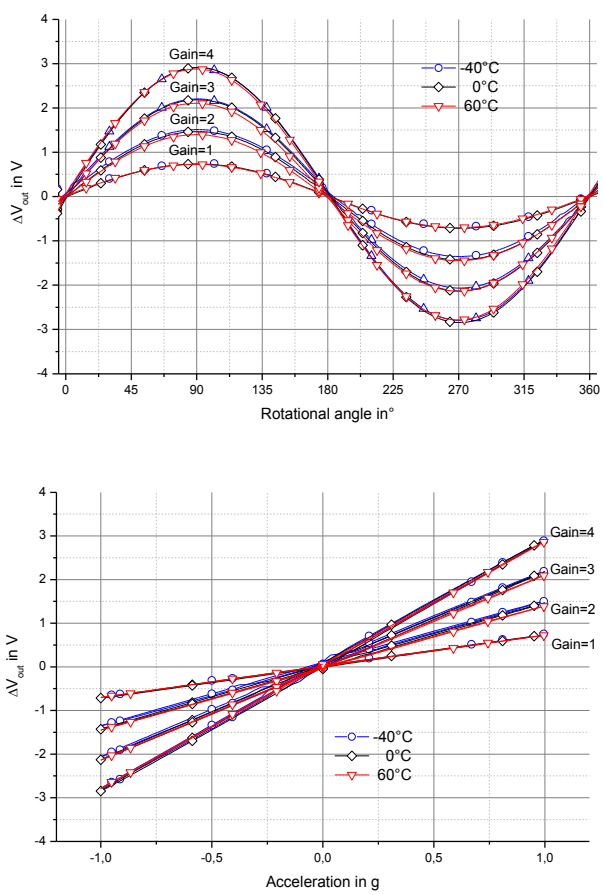

Fig. 6. *Measurement results: Output voltage over rotational angle (top) and output voltage over acceleration (bottom)*

III. TEST SETUP AND MEASUREMENT RESULTS

An automated test and characterization environment for acceleration measurement systems was developed at Fraunhofer IMS. A schematic drawing and a photo of the test setup are shown in Fig. 5. By the aid of a motorized rotary unit of type Trinamic TMCM-1140 accelerations in the range of ±1 g inside a climatic chamber model CTS-40/50 with well controlled temperature and humidity conditions are applicable. Temperatures between -40 °C and 120 °C can be applied and automatically controlled via an RS232 interface. The supply voltage of 5 V is generated by a programmable voltage source of type Agilent E3649A and the system clock by an arbitrary waveform generator (AWG) model Agilent 33250A. A square wave function with a frequency of 5 MHz, a duty cycle of 50 % and an amplitude of 3.3 V was applied as the system clock. The input impedance of the clock input was set to 50 Ω. The output voltages of the accelerometer system are measured using high precision digital multimeters (DMM) of type Keithley 2000.

The developed test PCB contains both the accelerometer

Copyright (c) 2018 IEEE. Personal use is permitted. For any other purposes, permission must be obtained from the IEEE by emailing pubs-permissions@ieee.org.

This is the author's version of an article that has been published in this journal. Changes were made to this version by the publisher prior to publication.
The final version of record is available at http://dx.doi.org/10.1109/JSEN.2018.2849873

MEMS and the ROIC which were mounted in CLCC44 housings. Further integrated components are used for a high precision voltage regulation (ADP3338AKC-5). The connection interfaces are SMC MULTICOMP - 26-09-TGG and SMC coaxial cables with length of 1 m or less are used. A PT100 temperature sensor with an accuracy of better than 0.3 K in a range from -100 °C and +100 C is also integrated and serves as reference element for temperature control. Its resistance is measured by a 4-wire measurement using a Keithley 2000 DMM and a built-in 20-channel scanner card.

Fig. 6 show the results of an angular rotation of the accelerometer (top) and for the calculated g-V curve (bottom). The measurements were performed with an angular step width of 2° in a range from -6° to 370°. The temperatures of -40 °C, 0 °C and 60 °C are applied with an accuracy of ±1 K. At each angular position the arithmetic mean of 100 measurements is shown. The output signals were measured for all four gain settings per angular position and temperature.

Noise measurements on the system outputs can be performed using high precision voltage amplifiers of type FEMTO HVA-200M-40-F. The amplifiers add an extra gain of 40 dB. This allows the measurement of very low noise levels which otherwise would be superposed by the analyzers self-noise. All connections to and from the amplifiers are made by shielded coax cables. The climatic chamber with its grounded chassis forms a good shielding against electrical interference from the environment. For low frequencies in the range from DC to several kHz, the noise amplitude density is measured using an FFT signal analyzer of type Agilent 35670A. The settings included a single initial calibration, a two channel instrument mode, AC coupling, a grounded input shield, deactivated weight filter, and an activated anti-alias filter. Spectrum analyzers for higher frequencies up to the GHz range are also available. Noise densities of less than 50 nV/$\sqrt{\text{Hz}}$ can be measured. Test execution and control of all measuring instruments is handled by a LabVIEW test software.

Noise measurements on only the ROIC are performed in the same measurement environment as those on the complete accelerometer. The sensing element was replaced by fixed capacitors of the same magnitude as the MEMS' nominal capacitance.

Fig. 7 shows the results for noise measurements of the developed accelerometer at room temperature and highest gain setting of 4. The resolution is 2 Hz and the measured values represent the arithmetic mean of 15 individual measurements.

The noise measurements were performed on an active vibration damped table whose effective damping lies in the

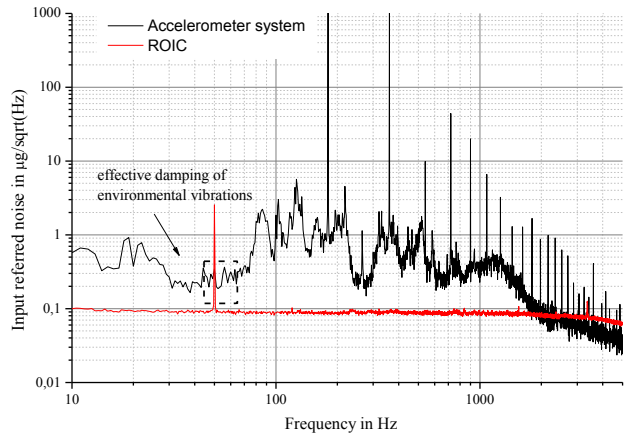

Fig. 7. *Measurement results: input referred noise of ROIC and Accelerometer*

frequency range of 30 Hz – 40 Hz. In this range, an acceleration equivalent noise level (AEN) of only 216 ng/$\sqrt{\text{Hz}}$ was measured. This is close to the theoretical value of 154 ng/$\sqrt{\text{Hz}}$, calculated for an electrical noise level of 50 zF/$\sqrt{\text{Hz}}$. It can also be seen that the total noise is significantly higher than the electrical noise generated by the ROIC, meaning that the sensing element is the limiting factor in this case. A next step for further improvement of the overall noise performance would be vacuum sealing of the MEMS.

The -3 dB bandwidth of the accelerometer was measured to be more than 5 kHz. This high bandwidth makes the sensor well suited for applications where high measurement accuracy over a wider frequency range is required, e.g. for the condition monitoring and predictive maintenance of rotary machinery [16] – [18].

The g-V curve (shown in the top curve of Fig. 6) shows a very linear correlation between acceleration and output voltage for all gain settings with a total harmonic distortion (THD) of only 1.1 %. Only small temperature sensitivity was measured with a sensitivity of less than 2 % within a temperature range from -40 °C to +60 °C (see Fig. 8 top).

The stability of the output was verified for a period of 30 h in a temperature controlled laboratory environment with a variation of 28.6 °C ± 0.24 K. The sensor system was accelerated with 0 g without any environmental damping. Previously, the system was conditioned for 24 h in the described environment. In Fig. 8 at the bottom the normalized

Copyright (c) 2018 IEEE. Personal use is permitted. For any other purposes, permission must be obtained from the IEEE by emailing pubs-permissions@ieee.org.

This is the author's version of an article that has been published in this journal. Changes were made to this version by the publisher prior to publication.
The final version of record is available at http://dx.doi.org/10.1109/JSEN.2018.2849873

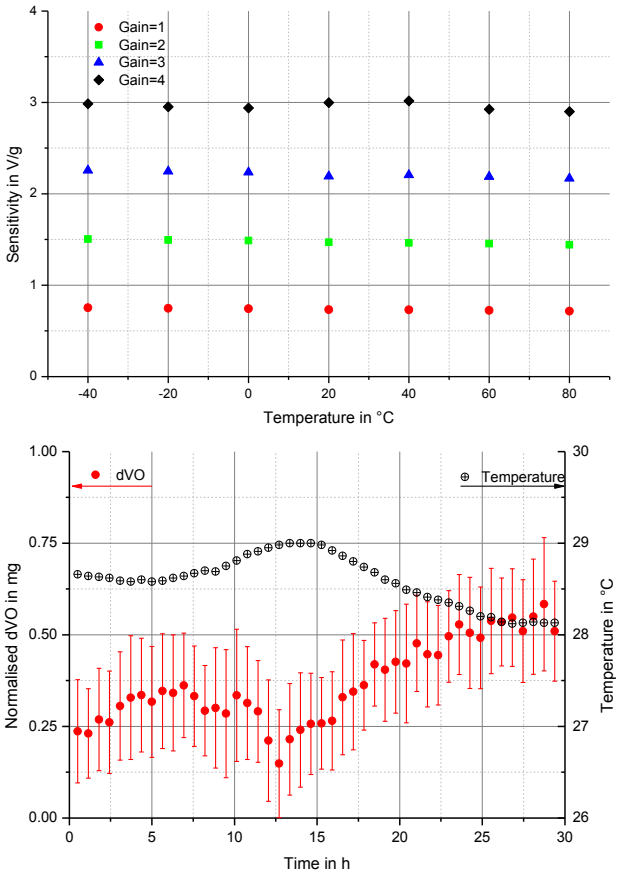

Fig. 8. *Measurement results: gain-dependet sensitivity over temperature (top) and output stability for 0 g acceleration (bottom)*

sensor signal is expressed in terms of acceleration. A temperature dependency is visible. For each measurement point the 1σ error obtained for 100 single measurements is shown. The mean 1σ error of all single measurements is 146 µg and the 1σ error over the whole period is 117 µg. Table 2 shows a comparison of the main parameters noise and bandwidth from this work with results from other groups published within the last years. All systems have single supply voltages in the range of 1.8 V to 7 V. Although similar noise performance has already been achieved with MEMS based solutions applying vacuum sealing of the sensing element, it has not yet been reached in combination with a measurement bandwidth of several kHz. This becomes even more obvious if we take the ratio of noise per bandwidth as a figure of merit, which is illustrated in the rightmost column of Table 2.

TABLE II
COMPARISON WITH SCIENTIFIC LITERATURE

Publication	Supply voltage in V	Noise floor in $\mu g/\sqrt{Hz}$	Bandwidth in Hz	Noise / Bandwidth in $ng/Hz^{3/2}$
This work	5	0.2	5k	0.04
[4]	7	0.2	300	0.67
[19]	5	0.3	300	1
[22]	±1.5	0.2	200	1
[20]	5	1.6	95	16.84
[21]	1.8	20.65	100	206.5

Additionally, MEMS based solutions like the ones presented in [4] apply vacuum sealing of the sensing element. This is not necessary in our case which makes the production process much simpler and cost efficient.

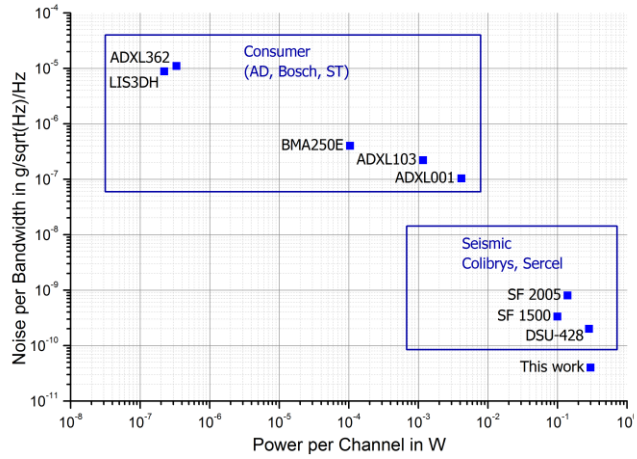

Fig. 9. *Benchmark with commercially available accelerometers*

Finally, Fig. 9 shows a benchmark of the presented sensor system with commercially available products. Systems developed for the consumer market (the top box in Fig. 9) typically focus on lower and lowest possible power consumption with reduced or moderate noise performance. Compared to those kinds of systems, the power consumption of the presented accelerometer (which was measured as 300 mW) is relatively high. Systems dedicated for seismic applications (lower right box) typically reach noise levels comparable to that reached in this work, but with significantly lower bandwidth and comparable power consumption.

IV. CONCLUSION

We presented the design and measurement results of a capacitive MEMS based accelerometer with focus on low noise and high measurement accuracy. The resulting noise performance is far below 1 $\mu g/\sqrt{Hz}$ which makes the accelerometer well suited for high precision applications such as seismic measurements. Comparisons have been made with systems presented in the scientific literature as well as commercially available products. It was demonstrated that, although systems with comparable noise performance are available, none of these solutions reach comparable high bandwidth of operation. Additionally, no special process steps, like vacuum sealing of the sensing element, are needed for the presented accelerometer. The standard CMOS and CMOS compatible production processes of the ROIC and the MEMS sensing element enable cost efficient manufacturing capability for mass production.

REFERENCES

[1] J. Bernstein, R. Miller, W. Kelley, and P. Ward, "Low-noise MEMS vibration sensor for geophysical applications," *Journal of Microelectromechanical Systems*, vol. 8, no. 4, pp. 433–438, Dec 1999.

[2] F. Chen, W. Yuan, H. Chang, I. Zeimpekis, and M. Kraft, "Low noise vacuum MEMS closed-loop accelerometer using sixth-order multi-feedback loops and local resonator sigma delta modulator," in *2014*

Copyright (c) 2018 IEEE. Personal use is permitted. For any other purposes, permission must be obtained from the IEEE by emailing pubs-permissions@ieee.org.

This is the author's version of an article that has been published in this journal. Changes were made to this version by the publisher prior to publication.
The final version of record is available at http://dx.doi.org/10.1109/JSEN.2018.2849873

IEEE 27th International Conference on Micro Electro Mechanical Systems (MEMS), Jan 2014, pp. 761–764.

[3] F. Rudolf, S. Gonseth, R. Brisson, and P. Krebs, "New generation of high performance/high reliability MEMS accelerometers for harsh environment," in *2014 IEEE/ION Position, Location and Navigation Symposium - PLANS 2014*, May 2014, pp. 7–11.

[4] H. Xu, X. Liu, and L. Yin, "A closed-loop $\Sigma\Delta$ interface for a high-q micromechanical capacitive accelerometer with 200 ng/ $\sqrt{\text{Hz}}$ input noise density," *IEEE Journal of Solid-State Circuits*, vol. 50, no. 9, pp. 2101–2112, Sept 2015.

[5] I. Sari, I. Zeimpekis, and M. Kraft, "A dicing free SOI process for MEMS devices," *Microelectronic Engineering*, vol. 95, pp. 121 – 129, 2012. [Online]. Available: http://www.sciencedirect.com/science/article/pii/-S0167931712000238

[6] N. Yazdi, F. Ayazi, and K. Najafi, "Micromachined inertial sensors," *Proceedings of the IEEE*, vol. 86, no. 8, pp. 1640–1659, Aug 1998.

[7] T. B. Gabrielson, "Mechanical-thermal noise in micromachined acoustic and vibration sensors," *IEEE Transactions on Electron Devices*, vol. 40, no. 5, pp. 903–909, May 1993.

[8] C. C. Enz and G. C. Temes, "Circuit techniques for reducing the effects of op-amp imperfections: autozeroing, correlated double sampling, and chopper stabilization," *Proceedings of the IEEE*, vol. 84, no. 11, pp. 1584–1614, Nov 1996.

[9] *Noise and Operational Amplifier Circuits*, Appl. note an-358 ed., Analog Devices.

[10] T. Yin, H. Yang, Q. Yuan, and G. Cui, "Noise analysis and simulation of chopper amplifier," in *APCCAS 2006 - 2006 IEEE Asia Pacific Conference on Circuits and Systems*, Dec 2006, pp. 167–170.

[11] C. C. Enz, E. A. Vittoz, and F. Krummenacher, "A cmos chopper amplifier," *IEEE Journal of Solid-State Circuits*, vol. 22, no. 3, pp. 335–342, Jun 1987.

[12] T. C. C. Kevin, D. Han, P. S. Ravinder, D. P. Duy, Y. P. Chin, W. L. Jian, D. Nuttman, and M. Je, "118-db dynamic range, continuous-time, opened-loop capactance to voltage converter readout for capacitive mems accelerometer," in *2010 IEEE Asian Solid-State Circuits Conference*, Nov 2010, pp. 1–4.

[13] J.-S. Goo, C.-H. Choi, A. Abramo, J.-G. Ahn, Z. Yu, T. H. Lee, and R. W. Dutton, "Physical origin of the excess thermal noise in short channel mosfets," *IEEE Electron Device Letters*, vol. 22, no. 2, pp. 101–103, Feb 2001.

[14] A. Utz, C. Walk, N. Haas, T. Fedtschenko, A. Stanitzki, M. Mokhtari, M. Görtz, M. Kraft, and R. Kokozinski, "An ultra-low noise capacitance to voltage converter for sensor applications in 0.35µm CMOS," *Journal of Sensors and Sensor Systems*, vol. 6, no. 2, pp. 285–301, 2017. [Online]. Available: https://www.j-sens-sens-syst.net/6/285/2017/

[15] W. M. Leach, "On the calculation of noise in multistage amplifiers," *IEEE Transactions on Circuits and Systems I: Fundamental Theory and Applications*, vol. 42, no. 3, pp. 176–178, Mar 1995.

[16] S. J. Lacey, "The role of vibration monitoring in predictive maintenance," Schaeffler (UK) Ltd, White Paper, 2010.

[17] S. J. Lacey, "An overview of bearing vibration analysis," *maintenance & asset management*, vol. 23, no. 6, pp. 32 – 42, November 2008.

[18] "Mechanical vibration – measurement and evaluation of machine vibration," Geneva, CH, November 2016.

[19] L. Aaltonen and K. Halonen, "Continuous-time interface for a micromachined capacitive accelerometer with NEA of 4 g and bandwidth of 300 Hz," *Sensors and Actuators A: Physical*, vol. 154, no. 1, pp. 46 – 56, 2009. [Online]. Available: http://-www.sciencedirect.com/science/article/pii/S0924424709003343

[20] N. Yazdi, H. Kulah, and K. Najafi, "Precision readout circuits for capacitive microaccelerometers," in *Proceedings of IEEE Sensors, 2004.*, Oct 2004, pp. 28–31 vol.1.

[21] C. K. Wang, C. S. Chen, and K. A. Wen, "A monolithic cmos mems accelerometer with chopper correlated double sampling readout circuit," in *2011 IEEE International Symposium of Circuits and Systems (ISCAS)*, May 2011, pp. 2023–2026.

[22] R. Abdolvand, B. Vakili Amini and F. Ayazi, "Sub-Micro-Gravity In-Plane Accelerometers With Reduced Capacitive Gaps and Extra Seismic Mass," in *Journal of Microelectromechanical Systems*, vol. 16, no. 5, pp. 1036-1043, Oct. 2007.

A. Utz received the Dipl.-Ing. degree in electrical engineering and electronics from the University of Dortmund, Germany in 2005 and the Dr.-Ing. degree from the University of Duisburg, Germany in electrical engineering in 2012.
From 2006 to 2008 he worked as a R&D engineer at Plastcontrol GmbH, a company which develops control systems for industrial process automation. Since 2008 he is with Fraunhofer IMS, first gaining his Dr.-Ing. degree and afterwards till now as a Research Associate in the field of Mixed Signal IC Design.

C. Walk received the B.Sc. and M.Sc. degrees from the University of Freiburg, Germany, in 2009 and 2012, respectively. He studied microsystems engineering at the University of Freiburg with a focus on optics and process technologies.
In 2012 he was a Research Assistant at Fraunhofer Institute for Solar Energy Systems (ISE), Freiburg, working in the field of optics and micro and nanostructured functional surfaces. Since 2012 he is with Fraunhofer IMS. From 2012 until 2014 he was a Research Assistant and since 2014 he is working as PhD student in the field of post-CMOS sensor development.

A. Stanitzki received the Diploma degree in electrical engineering from the Ruhr-University Bochum in 2008.
From 2007 to 20011 he worked at advICo microelectronics GmbH as an IC design engineer for RF-mixed-signal and radhard applications. Since 2012 he is leading the Mixed Signal IC Design group within Fraunhofer IMS, with a focus on energy harvesting medical implants, industrial precision sensor readout ICs and functional safety in analog ICs.

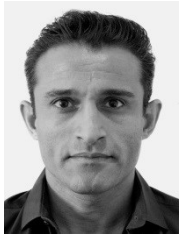

M. Mokhtari received the BEng degree in electronics engineering from the University of Southampton, UK in 2000 and the PhD degree in Microelectronics from the University of Southampton, UK in 2004, with a focus on oversampling sigma-delta modulators for advanced MEMS inertial sensors.
From 2004 to 2007 he worked as the Research Business Manager at Innos Ltd, UK developing and manufacturing rollable display technologies. He founded Mir Enterprises Ltd, UK in 2007 and holds the position of Managing Director to date. The company specialises in the design, fabrication and testing of micro and nano device technologies in both research and low volume manufacturing. He was appointed as a member of the advisory board at the London Technology Network from 2009 to 2010.

Copyright (c) 2018 IEEE. Personal use is permitted. For any other purposes, permission must be obtained from the IEEE by emailing pubs-permissions@ieee.org.

This is the author's version of an article that has been published in this journal. Changes were made to this version by the publisher prior to publication.
The final version of record is available at http://dx.doi.org/10.1109/JSEN.2018.2849873

M. Kraft currently is a Professor of Micro- and Nanosystems at the University of Leuven, Belgium, Department of Electrical Engineering/Micas group. From 2012-2015 he was a professor at the Montefiore Institute, University of Liege, Belgium and from 2012-2014, he was at the Fraunhofer IMS in Duisburg, Germany, where he headed the Department of Micro- and Nanosystems. He concurrently held the W3 Professorial Chair of Integrated Micro- and Nanosystems at the University of Duisburg-Essen. From 1999 to 2012 he was a faculty member and Professor of Micro-System-Technology at the University of Southampton, UK. He graduated with a Dipl.-Ing. (Univ.) in electrical and electronics engineering at the Friedrich Alexander Universität Erlangen-Nürnberg in 1993. In 1997 he was awarded a PhD from Coventry University, UK on the development of a MEMS accelerometer. He then spent two years at the Berkeley Sensors and Actuator Centre at the University of California working on integrated MEMS gyroscopes. His research interests include MEMS, micro- and nano-sensors and bio-engineering. He published over 250 papers as author and co-authors and serves as senior editor on IEEE Sensor Letters and Journal of Sensors and Sensor Systems as well on the technical program committee of ISSCC and several other conferences.

R. Kokozinski received the Dipl.-Ing. degree in electrical engineering in 1990 and the Dr.-Ing. degree in 1996, both from the University of Duisburg, Germany.
In 1990 he joined the Signal Processing and System Design Department at the Fraunhofer IMS, working in the area of analog and mixed analog-digital CMOS and BiCMOS IC design. From 1998 to 1999 he was with Toshiba Electronics Europe, Düsseldorf, Germany, where he headed the development of high-speed CMOS interface cells as well as the development of mixed-signal telecommunication ICs, e.g. for xDSL applications. He is now a Professor at the University Duisburg-Essen, Duisburg, Germany, and Head of the Integrated Circuits and Systems Department at Fraunhofer IMS. His research interests include design of microelectronic circuits and systems, analog and digital signal processing as well as design techniques for medical implants, functional safety, harsh environments and high temperature electronics.

Copyright (c) 2018 IEEE. Personal use is permitted. For any other purposes, permission must be obtained from the IEEE by emailing pubs-permissions@ieee.org.